Photoluminescence from liquid-exfoliated WS_2 monomers in polymer composites

Victor Vega-Mayoral,[1,2^] Claudia Backes,[3,4^] Damien Hanlon,[3,4] Umar Khan,[3,4] Zahra Gholamvand,[3,4] Maria O'Brien,[3,5] Georg S. Duesberg,[3,5] Christoph Gadermaier,[1,2] and Jonathan N. Coleman[3,4]*

[1]*Department for Complex Matter, Jozef Stefan Institute, Jamova 39, 1000 Ljubljana, Slovenia*

[2] *Jozef Stefan International Postgraduate School, Jamova 39, 1000 Ljubljana, Slovenia*

[3]*CRANN & AMBER, Trinity College Dublin, Dublin 2, Ireland*

[4]*School of Physics, Trinity College Dublin, Dublin 2, Ireland*

[5]*School of Chemistry, Trinity College Dublin, Dublin 2, Ireland*

^These authors contributed equally

*colemaj@tcd.ie

Abstract: While liquid phase exfoliation can be used to produce nanosheets stabilized in polymer solutions, very little is known about the resultant nanosheet size, thickness or monolayer content. Here we use semi-quantitative spectroscopic metrics based on extinction, Raman and photoluminescence (PL) spectroscopy to investigate these parameters for WS_2 nanosheets exfoliated in aqueous polyvinylalcohol (PVA) solutions. By measuring Raman and PL simultaneously, we can track the monolayer content via the PL/Raman intensity ratio while varying processing conditions. We find the monolayer population to be maximized for a stabilizing polymer concentration of 2 g/L. In addition, the monolayer content can be controlled *via* the centrifugation conditions, exceeding 5% by mass in some cases. These techniques have allowed us to track the ratio of PL/Raman in a droplet of polymer-stabilized WS_2 nanosheets as the water evaporates during composite formation. We find no evidence of nanosheet aggregation under these conditions although the PL becomes dominated by trion emission as drying proceeds and the balance of doping from PVA/water changes. Finally, we have produced bulk PVA/WS_2 composites by freeze drying where >50% of the monolayers remain unaggregated, even at WS_2 volume fractions as high as 10%.

Introduction

Over the last few years, the study of two-dimensional (2D) materials has become one of the most vibrant areas of nanoscience. Although this area was initially dominated by research into graphene, it has since broadened to encompass a wide range of 2D materials including boron nitride (BN), transition metal dichalcogenides (TMDs) such as MoS_2 and WSe_2, transition metal oxides (TMOs) such as MoO_3 and RuO_2 as well as a host of others including black phosphorous, silicene and germanane. These materials are extremely diverse and have been employed in a wide range of applications in areas from energy to electronics to catalysis.[1-5]

Two-dimensional nanosheets have been seen by many authors as ideal for inclusion in advanced composites. Nanoclay-polymer composites[6, 7] have been studied for decades while graphene has been widely explored as a filler in nanocomposites,[8, 9] particularly for mechanical reinforcement[10] and optical applications.[11-13] However, the broader family of inorganic 2D materials have only recently been targeted for composite applications. For example, both BN and MoS_2 have followed graphene as fillers for mechanical reinforcement of polymers,[14, 15] while MoS_2 has also been used as an additive to reduce wear and improve fire retardency in plastics[16, 17] and for photoactuation applications.[18] In addition, both MoS_2- and $MoSe_2$-filled composites have been used as saturable absorbers for the production of fiber lasers.[19-23]

For composite applications, because large quantities of 2D nanosheets are usually required, probably the most suitable nanosheet production method is liquid phase exfoliation (LPE). In this method, layered crystals, usually in powdered form, are exfoliated by ultrasonication[24, 25] or shear mixing,[26, 27] usually in appropriate solvents or surfactant solutions. After centrifugation to remove any unexfoliated powder, this method gives dispersions containing large quantities of high quality nanosheets. A significant advantage of this approach is its versatility; it has been used to exfoliate graphene,[24, 27-31] BN,[15] a range of TMDs[25, 26, 32, 33] and TMOs[34, 35] as well as black phosphorus[36-40] and a host of other 2D materials.[41, 42] Another advantage is the inherent processability of nanosheet dispersions. They can be fractionated to select nanosheets by size,[43] mixed with dispersions of other nanomaterials to create hybrids[25, 44] or fabricated into films or other structures.[3]

It is also very simple to produce polymer-based composites from nanosheet dispersions. In the applications described above,[14-23] the nanosheets were generally first exfoliated in

solvents or surfactant solutions and then mixed with polymer solutions. The resultant composite dispersions can then be cast or formed as required. However, an even simpler composite formation route has been described.[45, 46] Nanosheets can be exfoliated directly by sonication or shearing in polymer solutions.[27, 47, 48] Any exfoliated nanosheets are then coated with polymer chains and sterically stabilized against reaggregation.[48, 49] The resultant dispersions can be cast directly into composite films which have been studied for mechanical applications.[45, 46] However, exfoliation in polymer systems is still rather immature compared to LPE in solvents or surfactant systems. For example, while some work has been done to identify the rules relating polymer/solvent/nanosheet combinations,[48] no work has been done to study the effect of polymer concentration, centrifugation conditions or other processing parameters.

There are also other problems associated with composite formation, notably in relation to aggregation. If care is not taken, nanoscale fillers tend to aggregate during composite formation. This is particularly problematic for high aspect ratio 2D fillers which can show aggregation effects even at loading levels below 0.5%.[45, 46, 50, 51] Such aggregation is almost always detrimental to the properties of the composite, for example resulting in fall off in mechanical properties.[46] Alternatively for optical applications, well defined properties associated with monolayers might be required which would be destroyed by aggregation. This makes the ability to control aggregation during composite formation very important. To do this, it will first be necessary to routinely monitor the aggregation state of the filler particles. Such rapid and routine monitoring techniques are currently not available.

In this paper we address both the problem of the lack of detailed characterization of direct polymer exfoliation and the lack of rapid screening of the aggregation state. We used polyvinylalcohol (PVA) as model polymer system to study the liquid exfoliation of WS_2 in water. By using semi-quantitative spectroscopic metrics, we tracked nanosheet length, thickness and monolayer content during the exfoliation and post-exfoliation size-selection by centrifugation. When the monolayer content is increased by appropriate centrifugation conditions, we observe luminescence from monolayered nanosheets. The ability to use luminescence measurements of monolayered WS_2 allowed us to track whether aggregation occurs on drying, i.e. during composite formation. Importantly, while we observe a change in doping level of the nanosheets in the dried state, the luminescence from monolayered WS_2 is preserved even in composites with high WS_2 loading level.

Results and Discussion

Polymer Stabilized Nanosheets: Microscopy

To gain insights in liquid-exfoliation of TMDs using polymers as stabilizers, we have focused on WS_2 and PVA in water as model system. PVA/water is a well-known stabilizer and has been shown to exfoliate both graphene and BN nanosheets.[45, 46] We produced exfoliated WS_2 nanosheets by sonicating powdered tungsten disulphide (initial concentration C_i=30 g/L) in an aqueous solution of polyvinylalcohol (C_{PVA}=2 g/L) for 1 h. Any unexfoliated crystallites were removed by centrifugation, initially using two distinct sets of conditions utilizing relatively high and low rotation speeds. Under such conditions we would expect to achieve dispersions of relatively small and large nanosheets respectively.[43, 52]

The simplest way to characterize such dispersions is by extinction spectroscopy (usually referred to as absorption spectroscopy). As recently shown, this is a powerful technique for the characterization of liquid-exfoliated TMDs, as the spectra not only contain information on dispersed nanosheet concentration, but also on mean length and thickness of the exfoliated TMDs.[43] The length dependence is due to the effect of nanosheet edges on the spectral profile while quantum confinement effects result in well-defined shifts in A-exciton position with nanosheet thickness.

Shown in figure 1A are extinction spectra normalized to the local minimum measured for large and small PVA-stabilized WS_2 nanosheets. These spectra are typical of WS_2 and display the characteristic A-exciton at ~625 nm. The spectra are of slightly different shapes, consistent with the different lateral nanosheet sizes.[43] In addition, the A-exciton positions are slightly different from each other indicating that, in addition to differences in lateral size, the mean nanosheet thickness is different in each sample.[43]

Raman spectroscopy is an important tool for the characterization of liquid exfoliated nanosheets.[53-56] Usually, Raman spectroscopy is performed on nanosheets which have been deposited on a surface. However, here we performed Raman characterization directly on the dispersion. We achieved this by using a Raman spectrometer to probe individual droplets of WS_2 dispersion on a microscope slide. Typical spectra (excitation wavelength 532 nm) are shown in figure 1B for both large and small nanosheets. In addition to the characteristic Raman modes of WS_2 (e.g. the 2LA(M) at 352 cm^{-1}),[54, 56, 57] a broad peak is observed at ~2580 cm^{-1}

(617 nm, 2.00 eV). We attribute this peak to photoluminescence from monolayered WS_2.[53, 58] It is clear from this data that, when normalized to the main Raman mode at 352 cm^{-1}, the photoluminescence is considerably stronger for the dispersion of small nanosheets. While both monolayered and few-layered WS_2 will contribute to the Raman signal, only monolayers display any significant photoluminescence (PL). This means that the ratio of PL intensity to Raman intensity is related to the monolayer content in the dispersion. Because the PL/Raman ratios were I_{PL}/I_{Raman}=4% and 55% for large and small nanosheets respectively, this in turn implies that the monolayer content is considerably higher in the dispersion of smaller nanosheets.

In order to characterize the differences between the nanosheets in the dispersions, we deposited nanosheets both on holey carbon transmission electron microscopy (TEM) grids and Si/SiO_2 substrates for statistical TEM and atomic force microscopy (AFM) analysis. Typical TEM images of large and small nanosheets respectively are shown as insets in figure 1C-D. The lengths of a number of nanosheets in both dispersions were measured using TEM with histograms shown in figure 1 C-D. The nanosheet sizes were in the ranges 50-350 nm and 25-160 nm respectively for large and small nanosheets with corresponding mean nanosheet lengths of 120 and 60 nm,.

The determination of mean nanosheet length using statistical TEM is well established and reasonably straightforward. However, determination of the mean number of layers or monolayer content from AFM is more challenging. One obstacle is that stabilizers such as solvent, surfactant or polymer may contribute to the measured apparent AFM thickness so that nanosheets with a given number of layers appear thicker than their theoretical values. Thus, it is important to remove as much free polymer/surfactant as possible (such as by centrifuging the polymer/WS_2 dispersion at high speeds and redispersing the sediment in water). Then, as we have demonstrated previously,[27, 40, 42, 43] this problem can be overcome by analyzing the height of steps of incompletely exfoliated nanosheets allowing for a determination of number of layers from the measured AFM thickness. We note that care must be taken to only measure individually deposited nanosheets such as the ones in the images in figure 1B, D.

If these requirements are fulfilled, the number of layers of liquid-exfoliated nanosheets can be determined from statistical AFM analysis. The corresponding histograms for the WS_2-PVA samples are presented in figure 1 E-F for the large and small nanosheet samples respectively. The observed nanosheet thickness ranges were 1-17 and 1-8 monolayers per nanosheet with mean values of $\langle N \rangle$=6.1 and 3.1 layers for the large and small nanosheets

respectively. In addition to <N> it is possible to estimate the monolayer content from the AFM data. This can be represented as the number fraction or the volume fraction of monolayers. The monolayer number fraction, N_{ML}/N_T, was found to be 3.1% and 11% for the large and small nanosheets respectively. Furthermore, the monolayer volume fraction can be measured by AFM, as long as length, L, and width, W, are recorded simultaneously to the thickness, N, for each nanosheet and enough nanosheets are counted to be statistically relevant. Then the volume fraction is given by $V_f \approx \sum_{ML} LW / \sum_{All} NLW$. We have performed such an analysis and estimated the volume fraction of monolayers to be 0.3 % for the large nanosheets and 5.3 % for the small ones. We suggest that the measured PL intensity scales with the total volume of all monolayers probed by the laser beam while the Raman intensity scales with the total volume of all nanosheets. This implies the PL/Raman ratio should scale with V_f rather than the number fraction. To test this we calculated the ratio of PL/Raman, which we compare to both N_{ML}/N_T and V_f for both nanosheet samples. For large and small nanosheets, we found (PL/Raman)/(N_{ML}/N_T) to be ~1.3 and ~5 and (PL/Raman)/V_f to be ~13 and ~10 respectively. This is indeed consistent with the suggestion that $I_{PL} / I_{Raman} \propto V_f$.

Optimization of the polymer concentration

Above, we have demonstrated that WS_2 can be exfoliated and stabilized in aqueous PVA solutions with nanosheet size depending on the centrifugation conditions. However, the appropriate processing parameters remain unknown. In liquid phase exfoliation, the main parameters are initial concentration of WS_2 (C_i), processing/sonication time, t, power, P, and volume, V, as well as stabilizer concentration, C_{PVA}, and centrifugation conditions.[27, 59] As dispersed concentrations tend to scale monotonically with initial concentration and inputted energy density ($P \times t / V$),[27, 60] these parameters are important, but not very interesting. More interesting are the stabilizer concentration and centrifugation conditions as both these parameters tend to control not only the dispersed concentration but also the nanosheet size and so presumably the monolayer content.[26, 43, 52]

Since little is known about the effect of polymer concentration on either dispersed nanosheet concentration or size, we first studied the exfoliation for a range of PVA concentrations. Liquid-exfoliated WS_2 was prepared by sonicating WS_2 powder in a range of PVA-H_2O solutions with different C_{PVA}, followed by low-speed centrifugation (24.4 *g*, 12 h) to remove unexfoliated material (see methods). The resultant dispersions were characterized

by UV-Vis extinction spectroscopy with the normalized extinction spectra displayed in figure 2A for a range of C_{PVA}.

We found significant variations in the dispersed concentration of WS_2 as determined from the measured extinction according to the Beer-Lambert law using the extinction coefficient of liquid-exfoliated WS_2 (see SI, figure S1). The concentration of WS_2 nanosheets (figure 2B) was roughly constant at C_{WS2}~0.5 g/L for PVA concentrations up to C_{PVA}~3 g/L. However for higher PVA concentrations, C_{WS2} fell sharply. Similar behavior has previously been observed from anionic surfactant-exfoliated MoS_2 and was attributed to depletion interaction and charge screening.[59] While screening effects are unlikely to be important here, the depletion interaction may be relevant at high PVA concentrations. In addition, we suggest that the increased viscosity associated with higher polymer concentration may play a role. This suppresses motion during the sonication-based exfoliation thus reducing the efficiency of the exfoliation process ultimately leading to lower dispersed nanosheet concentration under equal sonication conditions.

As discussed above, extinction spectra of nanosheets contain information about mean nanosheet size and thickness. As previously shown for surfactant-exfoliated MoS_2 and to some extent WS_2,[43] the mean nanosheet length can be related to the peak intensity ratios in the optical spectra. In the case of WS_2, the ratio at the A-exciton / the local minimum at 290 nm, Ext_A/Ext_{290nm} appears are suitable choice as the spectral profile changes significantly (see figure 1A) for different nanosheet sizes. Here, we therefor refer to this parameter as the <L> metric. In addition, the mean nanosheet thickness is related the spectral position of the A-exciton, λ_A (determined from the second derivative, $d^2Ext/d\lambda^2$, as described in ref[43]). Here, we refer to λ_A as the <N> metric. Although the exact relationships between these metrics and the equivalent nanosheet dimensions has not yet been measured for WS_2 (as they have for MoS_2),[43] we can still use the <L> and <N> metrics as proxys for nanosheet length and thickness.

It is clear from figure 2A that the spectral profile does not show any significant changes with polymer concentration, indicating that C_{PVA} does not influence mean nanosheet size or thickness. This is confirmed by the plots in figures 2C and 2D showing the length and thickness metrics, respectively, to be invariant with PVA concentration. The data presented in figure 1 allows us to associate measured values of both <L> and <N> with two specific values of the length and thickness metric (dashed lines). This shows the dispersed nanosheets to be slightly below 120 nm long and ~6 layers thick for all PVA concentrations studied. This invariance of

nanosheet dimensions with PVA concentration is in stark contrast to recently reported results for the size and thickness of MoS_2 nanosheets exfoliated in aqueous surfactant solutions with varying surfactant content.[26] This is most likely due to differences in the mechanisms of polymer stabilization (steric) *versus* surfactant stabilization (electrostatic).[49]

In addition to measuring the mean nanosheet concentration, length and thickness as a function of process parameters, it is of great interest to gather information on the content of monolayers (MLs) produced in the exfoliation. As discussed above, we propose that this can be achieved for a nanosheet dispersion by measuring the Raman/PL spectra and using I_{PL}/I_{Raman} as a measure of the monolayer volume fraction.

The Raman and PL spectra (excitation wavelength 532 nm) were measured simultaneously on droplets as described above and in the methods section. The resultant spectra are shown in figure 2E normalized to the main Raman phonon (2LA(M) at 352 cm^{-1}). Although weaker than that shown in Figure 1, PL can clearly be seen around 2600 cm^{-1}. Figure 2F shows a magnification of the PL for a subset of the samples where wavenumber has been converted to wavelength. This clearly demonstrates that the PL/Raman ratio varies with C_{PVA}, indicating the monolayer volume fraction to depend on the PVA concentration. The I_{PL}/I_{Raman} ratio is plotted as a function of PVA concentration in figure 2G. It first increases with PVA concentration before falling off at PVA concentration >2 g/L, indicating the monolayer V_f to peak at C_{PVA}~2 g/L. Since we observed the dispersed WS_2 concentration to decrease with PVA concentration, it is also important to test whether the actual monolayer concentration also peaks at C_{PVA}=2 g/L. Because $I_{PL} / I_{Raman} \propto V_f$, the monolayer concentration is proportional to the product $(I_{PL} / I_{Raman}) \times C_{WS2}$. This parameter is plotted as a function of PVA concentration in figure 2H also showing a peak at a PVA concentration of 2 g/L. This means, in order to maximize monolayer content, a PVA concentration of 2 g/L is beneficial and hence chosen for the remainder of the study.

However, care must be taken with this analysis. In addition to affecting monolayer population, changes in PVA concentration may lead to different packing densities of PVA on the nanosheet surface, leading to changes in the dielectric constant which may have an impact on the observed PL intensity.[61] More detailed studies will be needed to clarify this.

We note that the PL measurements shown in figure 2 E-F were obtained without any size selection. This is in contrast to previous reports on photoluminescence of liquid-exfoliated

MoS_2 measured using a photoluminescence spectrometer.[43] In that case, without size-selection to increase the monolayer population, no PL was observed. This illustrates the advantages of using a Raman spectrometer to acquire PL spectra from the surface of a liquid drop.

Optimization of the post-exfoliation centrifugation

In order to improve the monolayer content in the dispersion and hence optimize the photoluminescence intensity, we performed size selection by controlled centrifugation with increasing centrifugation velocities in consecutive steps similar to procedures described previously.[27, 40, 42] Details are given in the methods section. This procedure has been shown to yield dispersions with varying mean size and thickness distributions and, as we will describe below, different monolayer volume fractions. The normalized extinction spectra (figure 3A) show expected changes in spectral features for the size-selected dispersions, consistent with both nanosheet size and thickness decreasing with increasing *g*-force. The length metric, Ext_A/Ext_{295nm} is plotted as function of mean centrifugal force in figure 3B illustrating significant variations in mean nanosheet lengths from >120 nm at low rotation rate to <60 nm at high rotation rate. Similarly, the thickness expressed *via* the A-exciton peak position, λ_A, in figure 3C also confirms the size selection with <N> falling with rotation rate from >6 at low rate to <3 at high rate.

To test whether the changes in length and thickness distributions coincide with different volume fractions of monolayers, the dispersions were subjected to liquid Raman/PL measurements. The resultant spectra are displayed in figure 3D and show that this is indeed the case. Values of I_{PL}/I_{Raman} of up to 1 (indicating relatively high monolayer populations) could be achieved by this simple centrifugation procedure. We plot the PL/Raman peak intensity ratio as a function of centrifugal force in figure 3E. The horizontal lines indicate the volume fraction of monolayers determined by AFM on two samples (see figure 1). The PL/Raman ratio, and so the monolayer V_f, increases with rotation rate but, interestingly, saturates for very high centrifugation speeds. This is somewhat unexpected and could be attributed to the fact that the nanosheets in this case are also very small (figure 3B) in lateral dimensions so that the photoluminescence of the monolayers is potentially quenched by edge-effects. This has previously been observed for very small liquid-exfoliated MoS_2 nanosheets.[43] We can observe the relationship between monolayer content and nanosheet size in figure 3F, where we plot I_{PL}/I_{Raman} as a function of the nanosheet length metric. This shows that to achieve monolayer V_f>5% means accepting monolayer length <60 nm.

Optical properties of WS_2 during drying

One of the great advantages of exfoliating nanosheets directly in polymer solutions is that the resultant dispersions can be used to form polymer-nanosheet composites simply by driving off the solvent.[45, 46] However, nanosheet aggregation during composite formation is always a significant problem. The ability to track the monolayer volume fraction using a Raman spectrometer allows us to probe aggregation effects during composite formation for the first time.

To do this, we have monitored the Raman/PL spectra of a liquid drop (C_{WS2}~0.1 g/L, C_{PVA}=2 g/L, $M_{WS2}/(M_{WS2}+M_{PVA}) \sim 5wt\%$) during drying at room temperature, measuring at 5 min intervals. A subset of the spectra is shown in figure 4A and B. The as-recorded, non-normalized spectra (figure 4A) show an increase in signal intensity as the drop dries (N.B. the shoulder at 3,330 cm^{-1} is the water Raman mode). This is because the concentration of WS_2 is increased as water evaporates so that more nanomaterial is sampled in each measurement. In turn, the spectra normalized to the 2LA(M) Raman mode (352 cm^{-1}) and plotted *versus* energy (figure 4B) reveal that changes in the shape of the WS_2 PL are observed as the drying proceeds. The PL decreases in intensity, broadens and becomes increasingly asymmetric. The drying/evaporation of water is furthermore reflected in the relative decrease of the water Raman mode at ~3,330 cm^{-1} (~1.9 eV when excited with 532 nm).

To further examine the spectral changes, the PL spectra (normalized to the Raman mode of WS_2) were fit to Gaussian lineshapes as shown for two spectra in figure 4C. The full set of spectra is shown in the SI (figure S2). Since nanosheets of different sizes and random orientation are sampled in each measurement, we find Gaussian fits more appropriate than Lorentzians due to inhomogeneous broadening. In all cases, the WS_2 PL can be described well by two Gaussians which we attributed to emission from excitons at ~ 2.01 eV and trions at slightly lower energy.[62-65] In addition, the water Raman peaks can be identified in the 0-15 min spectra where the drop is still wet. For simplicity, we also fit this set of water peaks to a single Gaussian.

In figure 4D we plot the energies of the exciton and trion as the water is evaporated. After 15-20 min, no signal from the water can be identified so that we conclude that the drop has mostly dried at that stage. This time is indicated by the grey vertical lines in the figure. The PL positions of both exciton (2.01 eV) and trion (1.99 eV) are relatively constant for the first 20 mins but begin to redshift once the water has mostly evaporated, saturating at 1.998 eV

(exciton) and 1.95 eV (trion), respectively after ~70 mins. We believe these shifts are associated with conformational changes of the polymer that occur as the water evaporates and the polymer either crystallizes or adopts an ideal chain conformation.[66] We expect such a rearrangement of the polymer on the nanosheet surface will lead to different levels of doping due to changes in the local chemical environment.

To confirm this, we also analyzed photoluminescence intensity, width and area as a function of drying time in figures 4E-G. The photoluminescence intensity of the exciton (figure 4E) dramatically decreases from 0.6 to 0.19 as the drop dries. Again, the dominant changes occur after the water Raman signal has disappeared (20 mins). Interestingly, the trion height stays approximately constant over the whole time period. As shown in figure 4F, this is accompanied by a broadening of the photoluminescence from both exciton and trion which likely reflect the changes in the dielectric constant around the nanosheets.[61]

In figure 4G, the PL areas of exciton and trion, as well as the summed area of both components are plotted *versus* time. This is of greatest relevance to understand whether reaggregation of the nanosheets is successfully prevented in the dried state due to the surrounding polymer. While the exciton area decreases, the trion area increases. Most importantly, the total PL area of both components stays broadly constant. This transfer of exciton photoluminescence to trion photoluminescence suggests an increase in the level of doping from the surrounding polymer in the dried state compared to the liquid state. This is best expressed as ratio of trion to exciton area in figure 4H showing an increase from the trion emission relative to the exciton emission by a factor of ~2. It is clear from this panel that the transfer of PL from exciton to trion only begins to occur once the water has mostly evaporated (20 mins) and is about to saturate by the time 80 minutes have passed.

We rationalize these observations as follows. PVA can act as *n*-type dopant for the WS_2 (i.e. electron donor due to the -OH groups). However, in the liquid state, this is partly overcompensated by the surrounding water acting as *p*-type dopant giving initial trion/exciton areas of ~1.[61, 67] As the water is evaporated, the actual *n*-type doping effect of PVA begins to dominate, resulting in broadened, red-shifted photoluminescence and an increased trion/exciton ratio. While the water has mostly evaporated after 20 minutes, we suggest that there is a residual portion of water, perhaps interacting strongly with the PVA, which evaporates more slowly over the 20-80 minute period. As this residual water evaporates, both the doping level and the polymer conformation change, resulting in the observed changes in PL.

We have confirmed that these changes in the WS_2 PL are indeed related to the presence of H_2O-PVA and PVA rather than random restacking of the nanosheets by analyzing the photoluminescence of vapor-grown WS_2 before and after deposition of a liquid drop of PVA and after evaporation of the water. Qualitatively, exactly the same result is obtained as summarized in the SI figure S3-5 and table S1. Similar to the situation in solution, we observe an increase in the trion emission relative to the exciton emission as a drop of H_2O-PVA is placed on the CVD-grown WS_2. This is accompanied by a slight broadening of both the exciton and the trion. These spectral changes become even more prominent as the water is evaporated confirming the strong *n*-type doping from the PVA.

While it is clear that the PL/Raman intensity is decreased in the dried compared to the liquid state due to the reduced exciton emission, it is very important to note that the PL area stays mostly constant. This suggests that the nanosheet-nanosheet aggregation is indeed successfully prevented by the polymer surrounding of the exfoliated nanosheets, at least at this mass fraction of ~5%. In addition, the drying experiment emphasizes that liquid-exfoliated TMDs are ideal model systems to study the impact of molecules and polymers on the optical properties.

Production of luminescent WS_2-PVA composites

The knowledge that the WS_2 nanosheets do not catastrophically aggregate during drying of WS_2-PVA dispersions suggests that it should be possible to produce solid WS_2-PVA composite films with monolayer content which is high enough for the composite to be luminescent. To investigate this, we prepared WS_2-PVA composites in two different ways. Firstly, we applied standard solution processing techniques, casting the WS_2-PVA dispersion into a Teflon mold and drying at 328 K in a vacuum oven for 24 h (see methods). This gave a shiny, transparent, bright yellowish-greenish colored film (figure 5A left). Alternatively, we prepared composites from the same dispersion by freeze-drying.[68] This gives soft, foam-like structures of a duller green color (figure 5A right). In both cases, polymer and WS_2 concentrations were adjusted to C_{PVA} = 30 g/L and C_{WS2} = 0.31 g/L to yield composites with a mass loading of 1.1 wt% of WS_2. In both cases, the composites looked quite uniform with no visual evidence of WS_2 aggregation. These as-produced polymer composites were subjected to Raman/PL measurements. Unfortunately, even though we reduced the laser power to 0.02 mW, the spectra were dominated by heating effects due to the low thermal conductivity of the PVA matrix (SI, figure S5).

To reliably acquire PL/Raman spectra from the polymer composite, we found it necessary to increase the WS_2 mass fraction to 10wt% (C_{PVA} = 30 g/L and C_{WS2} = 3 g/L). Under normal circumstances, such high filler loading would generally lead to aggregation during drying.[50] However, composite formation by freeze-drying should result in reduced aggregation. In freeze drying of polymers, solvent removal occurs so rapidly that the chains may not even have time to entangle.[69] By analogy, we do not expect the nanosheets to have time to aggregate but rather to remain surrounded by polymer chains. The resultant composite is shown in the inset of figure 5B and is a much darker color than before due to the higher WS_2 loading level. The Raman/PL spectrum of a freeze-dried WS_2-PVA composite (average of 100 spectra measured with 0.2 mW laser power) is displayed in figure 5B. The WS_2 PL is clearly discernible with a PL/Raman peak intensity ratio of ~0.25. This indicates that considerable numbers of individual nanosheets remain unaggregated even at very high WS_2 loading levels.

A great advantage of the foam-like freeze dried composites is that they can be readily redispersed in water by mild sonication (5 min in sonic bath). An example of a redispersed composite is shown in the photograph in the top inset in figure 5C. On the left is a WS_2/PVA composite directly after immersing it in water and on the right after 5 min of bath sonication by which time it has completely redispersed. The extinction spectrum of the redispersed composite is shown in figure 5C and is nearly identical to the spectrum of the starting dispersion. The bottom inset shows the A-exciton position to be virtually unchanged after redispersion, showing the mean nanosheet thickness to be the same in the redispersed and original dispersion. This is further confirmed by Raman/PL spectra in figure 5D showing the photoluminescence spectrum of the redispersed composite to be virtually identical to that of the starting composite. This shows that whatever the aggregation state of the nanosheets in the polymer matrix, they can be very easily redispersed and returned to their original dispersed state. Consequently, any aggregation that does occur could not result in any strongly bound structures.

Finally, figure 5D shows the PL area in the composite to be 52% of that for the dispersion used to prepare the composite (both normalized to the Raman peak at 352 cm^{-1}). This implies that during composite formation (drying), even for this high mass fraction (10 wt%), bulk composite, approximately half the WS_2 monolayers remain unaggregated. It is worth noting that, while it is important to observe that the monolayer aggregation is not as severe as might be expected, this result does not tell us anything about the aggregation of few-layer nanosheets (because they are not luminescent). It is entirely possible that few-layers may aggregate at a

significantly greater rate than monolayers. More work will be required to investigate this. In addition, we believe the low levels of monolayer aggregation may be largely due to the rapidity of composite formation during freeze drying and may not be replicable using standard composite formation techniques.

Conclusion

In summary, we have studied the exfoliation of WS_2 in aqueous PVA solutions where PVA is chosen as a model polymeric stabilizer. The effect of both polymer concentration and centrifugation conditions on dispersed concentration, nanosheet length, thickness and monolayer volume fraction were studied by the aid of semi-quantitative spectroscopic metrics based on extinction and Raman/photoluminescence spectra. After optimization of PVA concentration, we obtained dispersions with monolayer volume fractions of >5 % and easily observable photoluminescence.

This allowed us to study the behavior of monolayers during film formation by slow solvent evaporation. By monitoring Raman/PL spectra of the dispersion on drying, we were able to show that the PVA leads to *n*-type doping of the nanosheets as manifested by an increased emission of the trion luminescence. Importantly, the photoluminescence of the monolayer is not quenched in the dried state due to efficient shielding of the randomly restacked nanosheets.

Finally, we fabricated WS_2-PVA composites by both standard composite formation and freeze drying. We showed that the monolayer PL of the WS_2 is retained, but broadened and asymmetric in the freeze-dried composites with high WS_2 loading levels of 10 wt%. These composites are readily redispersible in water leading to a complete restoration of the spectral features. We expect these composites to be of interest for a number of studies on the optical properties of TMDs such as saturable absorbers[70] or second harmonic generators.[71] In addition, our results show that the ability to make ML-rich TMD dispersions offers exciting perspectives to study interactions with surrounding molecules and doping effects.

Materials and Methods

Materials

WS_2 and polyvinyl alcohol (PVA) were purchased from Sigma Aldrich at the highest available purity and used as received.

Exfoliation

Liquid-exfoliated WS_2-PVA dispersions were obtained by immersing WS_2 powder (initial concentration, C_i = 30 g/L) in 20 mL of aqueous PVA solutions with PVA concentrations as quoted in the main text. The mixture was sonicated under ice-cooling with a tapered microtip (Sonics VX-750) for 1 h at 35 % amplitude with a pulse of 6 s on and 2 s off. For the dispersion study with varying the PVA concentrations, the resultant dispersion were centrifuged at 500 rpm (24.4 *g*) for 12 hours to remove unexfoliated WS_2. This long centrifugation was required, as the viscosities in the samples due to the varying polymer concentrations were significantly different leading to different sedimentation velocities. For the remainder of the study, the PVA concentration was fixed to 2 g/L.

Size selection

To select nanosheets by size, we used controlled centrifugation with sequentially increasing rotation speeds as previously reported.[27, 42] An initial centrifugation at 0.5 krpm (24.4*g*, 1.5 h) was performed to remove unexfoliated material. The supernatant was subjected to further centrifugation at 2 krpm (390*g*, 1.5 h). The sediment was collected in fresh water-PVA (N.B., this samples was subjected to AFM), while the supernatant was subjected to further centrifugation at 3.5 krpm (1,193*g*, 1.5 h). Again, the sediment was collected and the supernatant centrifuged at higher rpm. This procedure was repeated for 5krpm (2,436*g*, 1.5 h), 7,5 krpm (5,478.8*g*, 1.5 h), 10 krpm (9,744*g*, 1.5 h) and 15krpm (21,924*g*, 1.5 h) to yield samples with decreasing sizes in the respective sediments. Compared with a method based on taking the supernatant from a single step centrifugation, this produces dispersions with lower polydispersity, as both smaller and larger nanosheets are removed from a given size-selected dispersion. This greatly facilitates microscopic characterization required to accurately determine length and thickness. In addition, the volume can be reduced in the redispersion step facilitating Raman/PL measurements on liquid drops. In this case, the sediment of 3 mL of the original dispersion was redispersed in 1.5 mL in order to increase the concentration. The data presented in figure 2 uses the central rpm/*g*-force to express average over two consecutive centrifugation steps. For example, the sediment collected from the 2 krpm centrifugation has a central rpm of 1.25 krpm (152 *g*).

Composite formation

Since a larger quantity of exfoliated WS_2 is required to prepare the composites, exfoliation and size selection was up-scaled to larger volumes as follows: WS_2 powder (initial concentration, C_i = 30 g/L) was immersed in 80 mL of aqueous PVA solution (C_{PVA}= 2g/L). The mixture was sonicated under ice-cooling in a metal beaker by probe sonication using a solid flathead tip (Sonics VX-750) for 1 h at 60 % amplitude with a pulse of 6 s on and 2 s off. The dispersion was centrifuged in 15 mL aliquots using 28 mL vials in a HettichMikro 220R centrifuge equipped with a fixed-angle rotor 1016 at 5 krpm (2436 *g*) for 1.5 h. The supernatant was discarded and the sediment collected in 80 mL of fresh PVA (C_{PVA}= 2g/L) and subjected to a second sonication using a solid flathead tip (Sonics VX-750) for 5 h at 60 % amplitude with a pulse of 6 s on and 2 s off. From our experience, this two-step sonication procedure yields a higher concentration of exfoliated WS_2 and removes impurities. Size selection was performed as described above discarding the sediment of a 1.5 h centrifugation at 2436 *g*, subjecting the supernatant to a 1.5 h centrifugation at 9744 *g* and collecting the sediment of this centrifugation step. This sample was also subjected to AFM.

The as-obtained dispersion was used to fabricate freeze-dried and conventional composites. We chose 0.2 wt% WS_2 because, from a mechanical point of view in literature the optimal mechanical properties for layered nanofillers have been observed in the region of 0.2 wt%.[45, 46] However such a low concentration of WS_2 produces samples where thermal effects introduce a big background signal that mask the Raman or PL signal from WS_2. We have therefore tested final concentrations of 1.1 and 10 wt % of WS_2 for this study. The starting PVA concentration was constant for all the samples (C_{PVA}=30g/L) and the different WS_2 concentrations were achieved by diluting the original dispersion.

The classical polymer composites were obtained by pipetting 7 mL of the final dispersions in a Petri dish of 53 mm diameter. Petri dishes were placed in a vacuum oven at 328 K for 24 hours. Homogeneous non-scattering free standing composites films were obtained. In order to make the freeze-dried samples, porous scaffold freeze drying (FreeZone Triad, Labconco, KC, USA) was used. The dispersion was frozen to −30 °C (1 °C min^{-1}) and maintained at that temperature for 1 h. The temperature was then ramped up to −10 °C to increase the sublimation rate and held for 24 h under vacuum before being increased to room temperature.

CVD WS_2

Chemical vapor deposition of WS_2 was carried out in as previously described[72]. Briefly, WO_3 precursor patterns of 10 nm thickness were sputtered from a solid target (MaTecK GmBH). The patterns were deposited onto commercially available silicon dioxide (SiO_2, ~290 nm thick) substrates, which were thermally grown on top of <100> oriented crystalline Si wafers. The oxide deposition rate and thickness were monitored using a quartz crystal microbalance. The WO_3 precursor substrates were placed face up in a ceramic boat with a blank SiO_2 on Si substrate face down on top of them, in order to direct growth onto the top, blank substrate. The boat loaded into the hot zone, and heated to 750 °C. Sulfur vapour was produced by heating sulfur powder (MaTecK, 99%) to ~120 °C in an independently controlled upstream heating zone of the furnace, and transported to the samples using 150 sccm Ar carrier gas for 20 minutes. After sulfurization, the samples were annealed for 20 min at 750 °C and cooled down to room temperature.

Characterization and Equipment

Unless otherwise noted, a Hettich Mikro 220R centrifuge equipped with a fixed-angle rotor 1195-A and 1.5 mL vials was used. For this centrifuge and this rotor, the centrifugation rate, f is related to the centrifugal force via $RCF = 97.4\, f^2$where f is the rotation rate in krpm.

Optical extinction was measured on a Varian Cary 50 in quartz cuvettes with a pathlength of 0.4 cm. If necessary, the dispersions were diluted by aqueous PVA solution with equal PVA concentrations immediately prior to the measurement to yield optical densities below 1.5.

Raman and photoluminescence spectroscopy was performed on the liquid dispersions using a Horiba Jobin Yvon LabRAM HR800 with 532 nm excitation laser in air under ambient conditions. The Raman/PL emission was collected by 100× objective lens (N.A. = 0.8) and dispersed by 600 gr/mm with 25 % of the laser power (~5 mW). We did not find heating effects to occur even at this comparably high laser power when measuring in liquids. However, the laser focus had a dramatic impact. The following procedure was used to ensure reproducibility: A drop (~ 40 μL) was placed on a glass slide and the drop edge was optically focused using a 10 x objective. The focus for the measurement with the 100 x objective was readjusted in such a way that the laser was focused slightly above the drop. Focusing inside the drop lead to innerfilter and reabsorption effects causing the WS_2 PL to be asymmetric. We also note that measurements taken close to the drop edge were more reliable than in the center of the drop because the focus remained constant throughout the measurement due to the lower curvature of the drop and hence negligible changes in the focus by evaporation of water. The average of

~ 5 measurements are displayed. To follow the drying of a drop, 10 % of the laser power was used to avoid sample heating in the dried state. The laser was switched off after a measurement was acquired and the focus was readjusted prior to each measurement.

Bright field transmission electron microscopy imaging was performed using a JEOL 2100, operated at 200 kV while HRTEM was conducted on a FEI Titan TEM (300 kV). Holey carbon grids (400 mesh) were purchased from Agar Scientific and prepared by diluting dispersion to a low concentration and drop casting onto a grid placed on a filter membrane to wick away excess solvent. Statistical analysis was performed of the flake dimensions by measuring the longest axis of the nanosheet and assigning it "length".

Atomic force microscopy (AFM) was carried out on a VeecoNanoscope-IIIa (Digital Instruments) system equipped with a E-head (13 μm scanner) in tapping mode after depositing a drop of the dispersion (10 μL) on a pre-heated (100 °C) Si/SiO_2 wafer with an oxide layer of 300 nm. After deposition, the wafer was rinsed with 5 mL of water and 5mL of isopropanol. The wafer was the soaked in water overnight to remove residual PVA. Typical image sizes were 3x3 μm at scan rates of 0.4-0.6 Hz. The apparent thickness was converted to number of layers using previously elaborated step-height analysis of liquid-exfoliated nanosheets.[43]

Acknowledgement

The research leading to these results has received funding from the European Union Seventh Framework Program under grant agreement n°604391 Graphene Flagship. We have also received support from the Science Foundation Ireland (SFI) funded centre AMBER (SFI/12/RC/2278**).** In addition, JNC acknowledges the European Research Council (SEMANTICS) and SFI (11/PI/1087) for financial support. VV-M and CG acknowledge Marie Curie ITN network "MoWSeS" (grant no. 317451). CB acknowledges the German research foundation DFG (BA 4856/1-1). M.O. acknowledges an Irish Research Council scholarship via the Enterprise Partnership Scheme, Project 201517, Award 12508. G.S.D. acknowledges support from the SFI (PI_10/IN.1/I3030).

Supporting information is available and includes measurement of the extinction coefficient, fitted luminescence spectra and the impact on optical properties of PVA on CVD-grown WS_2.

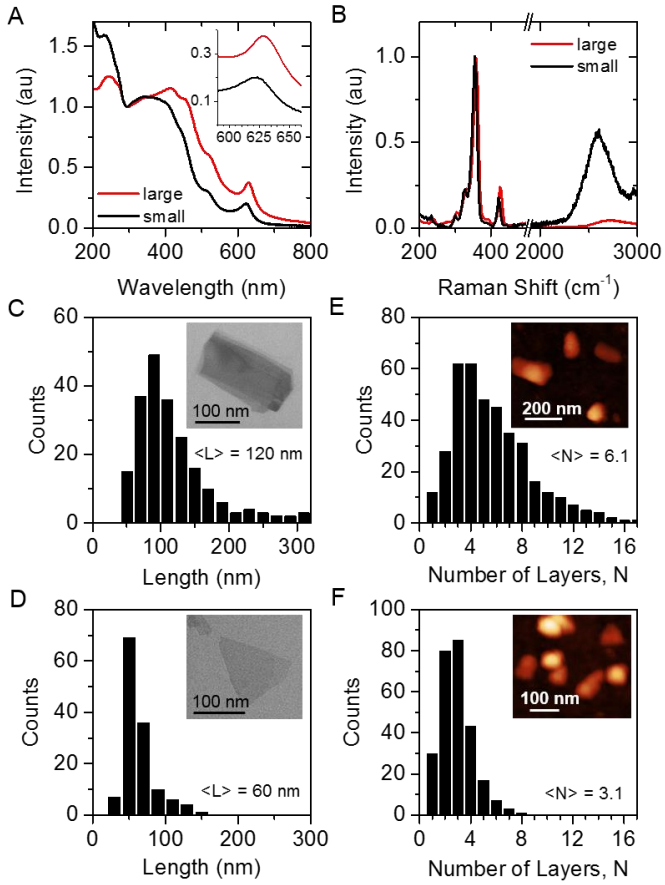

Fig. 1: A) Optical extinction spectra (inset: zoom-in of the A-exciton) and B) Raman/PL spectra of dispersions of PVA-stabilized WS_2 nanosheets produced using two different centrifugation regimes resulting in large and small nanosheets. C-F) Statistical microscopic analysis of PVA-stabilized WS_2 nanosheets. Insets show representative images. C-D) TEM length histograms for large and small nanosheets respectively. E-F) AFM thickness histogram (expressed as number of monolayers, N, per nanosheet) for large and small nanosheets respectively.

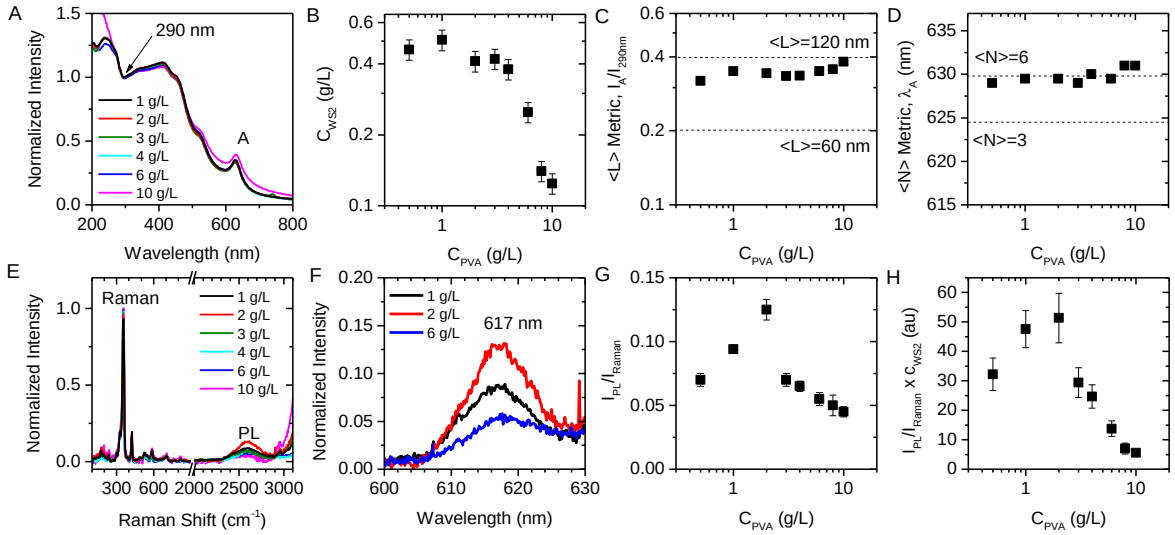

Figure 2: A) Normalized extinction spectra of WS_2 (initial concentration C_i = 30 g/L) exfoliated in PVA-H_2O with different concentrations of PVA, C_{PVA} after mild centrifugation (centrifugation speed 24 *g*, 12 h). No spectral changes are observed suggesting that the nanosheets have similar size and thickness distributions. B) Plot of dispersed WS_2 concentration as a function of PVA concentration. C) Length metric expressed as the extinction intensity ratio of the A-exciton / local minimum as a function of PVA concentration showing no significant changes. The dashed lines indicate values of length metric for which nanosheet length has been measured by TEM. D) Thickness metric expressed as the peak position of the A-exciton as a function of PVA concentration also showing no changes in thickness. The dashed lines indicate values of thickness metric for which nanosheet thickness has been measured by AFM. E) Raman/photoluminescence spectra (λ_{exc}= 532 nm) of WS_2 exfoliated in PVA-H_2O with different concentrations of PVA normalized to the main Raman mode. F) Zoom-in of the photoluminescence for a subset of the samples showing PL from monolayered WS_2 at 617 nm. G) Plot of photoluminescence / Raman intensity as a function of PVA concentration. This ratio provides a qualitative metric for the volume fraction of monolayers and shows a peak at C_{PVA} of 2 g/L. H) Plot of photoluminescence / Raman intensity multiplied by the dispersed concentration of WS_2 being indicative for monolayer yield as a function of PVA concentration.

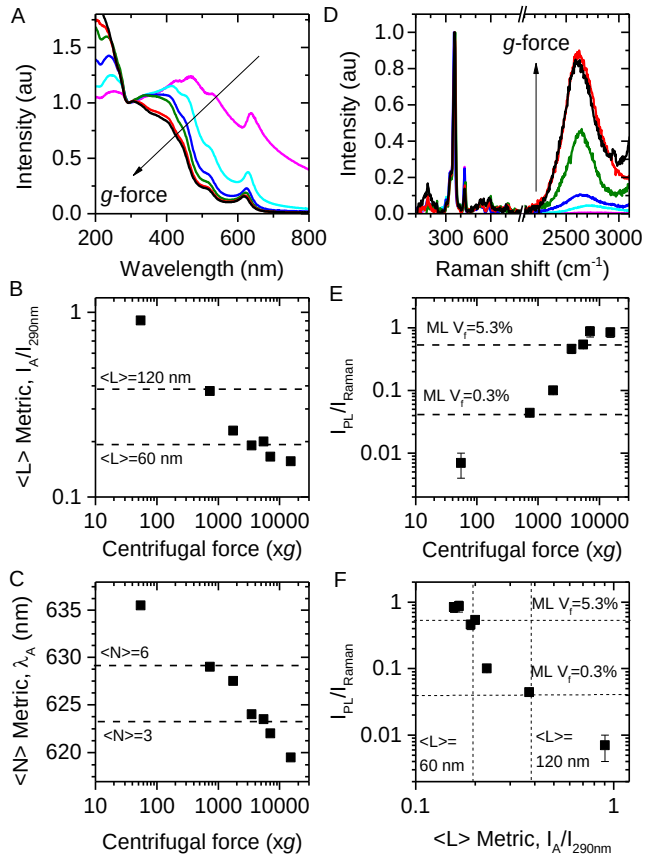

Fig. 3: A) Normalized extinction spectra of WS_2 exfoliated in PVA-H_2O (C_i= 30 g/L, C_{PVA}= 2 g/L) after centrifuging at different rotational speeds (1.5 h each step) showing characteristic changes in the spectral shape reflecting different sizes and thicknesses obtained. B) Length metric expressed as the extinction intensity ratio of the A-exciton / local minimum as a function of the centrifugal force. The dashed lines indicate values of length metric for which nanosheet length has been measured by TEM. C) Thickness metric expressed as the peak position of the A-exciton as a function of the centrifugal force. The dashed lines indicate values of thickness metric for which nanosheet thickness has been measured by AFM. D) Raman/photoluminescence spectra (λ_{exc}= 532 nm) of WS_2 exfoliated in PVA-H_2O after centrifuging at different rotational speeds. The relative PL intensity, i.e. the volume fraction of monolayers increases as the centrifugal force is increased. E) Plot of photoluminescence / Raman intensity as a function of centrifugal force. The dashed lines indicate values of ML volume fraction metric for which nanosheet thickness has been measured by AFM. F) Plot of photoluminescence / Raman intensity as a function of nanosheet length metric with measured values of each metric shown as dashed lines.

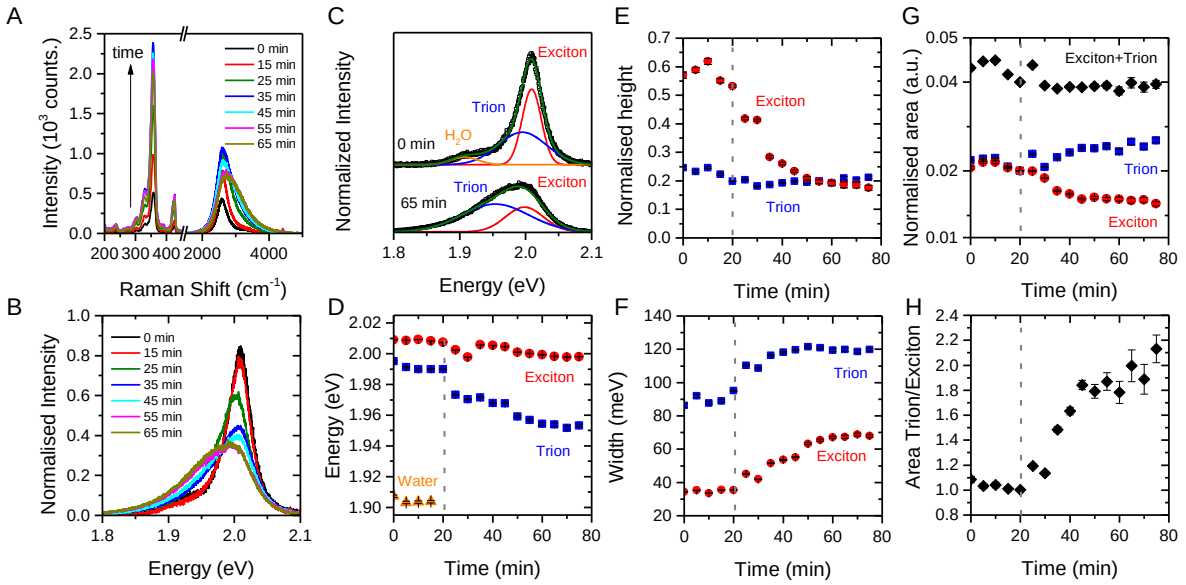

Fig. 4: A) Evolution of the Raman/PL spectra of small WS_2-PVA during drop drying. The figure legend indicates the time in minutes. As the drop dries, the concentration is increased leading to more nanosheets being sampled during the measurement hence increasing the signal intensity. B) Evolution of the PL spectra plotted *versus* energy after normalization to the Raman mode during drop drying. As the drop dries, the PL of WS_2 becomes lower in intensity, broadens and becomes more asymmetric. C) The PL spectra can be fit with two (dried) or three (dispersion) Gaussian lineshapes, respectively, as exemplarily shown for two spectra. We attribute the components to emission from the exciton at highest energy, trion and slightly lower energy and Raman scattering from water at ~1.9 eV as indicated. D) Evolution of exciton and trion energies as a function of time from fitting the spectra as shown in C. The water has evaporated after ~20 min as indicated by the grey vertical line. Both exciton and trion energy decreases further after all water has evaporated before saturating at lower energies. We attribute this intermediate regime to conformational changes of the polymer. E) Exciton and trion peak heights as a function of time. The trion intensity is widely constant, while the exciton intensity falls off. F) Plot of exciton and trion peak widths as a function of time. Both components broaden in the dried state. G) Plot of exciton, trion and total PL area *versus* time. While the exciton area decreases, the trion area increases after evaporation of the water. Importantly, the total area stays roughly constant confirming that the monolayer properties are preserved in the composite, i.e. reaggregation is successfully prevented from the polymer. H) Plot of trion/exciton area showing an increase of the trion/exciton ratio of a factor of 2. This strongly suggests n-type doping from the PVA.

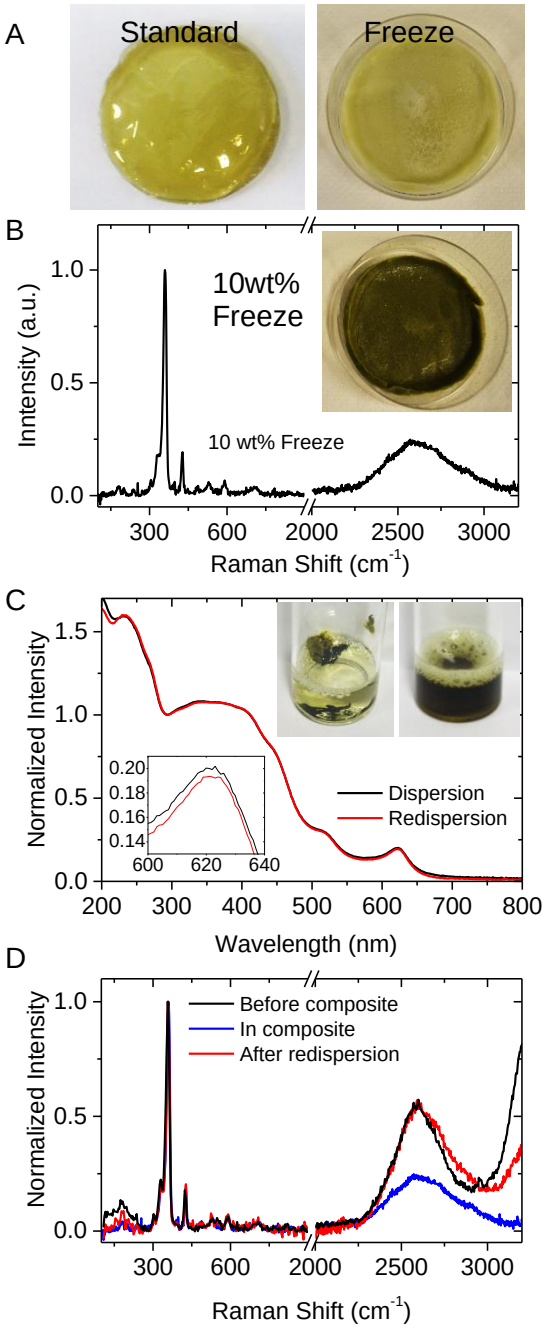

Fig. 5: A) Photographs of WS_2-PVA (1.1 wt% WS_2 loading) composites obtained by means of classical composite preparation (water evaporation by heat/vacuum) and by freeze drying. NB: The loading level of WS_2 was too low to reliably acquire Raman/PL spectra due to heating effects from the polymer. B) Raman/PL spectrum of a freeze-dried WS_2-PVA composite with 10 wt% of WS_2 (mean of 100 spectra measured with 0.2 mW laser power). Inset: photograph of the composite. C) The freeze-dried composites can be readily redispersed in water by 5 min bath sonication. No changes in the extinction spectra before (black) composite formation and after redispersion (red) are observed. Top inset: photographs of the vials after immersing the

composite into water (left) and after 5 min of bath sonication (right). Bottom inset: Zoom of the A-exciton. D) Raman/PL spectra of WS_2-PVA as exfoliated, in the freeze-dried composite and after redispersion of the composite. The PL is completely recovered.

References

[1] M. Chhowalla, H. S. Shin, G. Eda, L.-J. Li, K. P. Loh, H. Zhang, Nature Chemistry 2013, 5, 263.
[2] A. K. Geim, I. V. Grigorieva, Nature 2013, 499, 419.
[3] V. Nicolosi, M. Chhowalla, M. G. Kanatzidis, M. S. Strano, J. N. Coleman, Science 2013, 340, 1420.
[4] Q. H. Wang, K. Kalantar-Zadeh, A. Kis, J. N. Coleman, M. S. Strano, Nature Nanotechnology 2012, 7, 699.
[5] K. S. Novoselov, V. I. Fal'ko, L. Colombo, P. R. Gellert, M. G. Schwab, K. Kim, Nature 2012, 490, 192.
[6] Y. Kojima, A. Usuki, M. Kawasumi, A. Okada, Y. Fukushima, T. Kurauchi, O. Kamigaito, J. Mater. Res. 1993, 8, 1185.
[7] S. Pavlidou, C. D. Papaspyrides, Progress in Polymer Science 2008, 33, 1119.
[8] X. Huang, X. Qi, F. Boey, H. Zhang, Chemical Society Reviews 2012, 41, 666.
[9] H. Kim, A. A. Abdala, C. W. Macosko, Macromolecules 2010, 43, 6515.
[10] R. J. Young, I. A. Kinloch, L. Gong, K. S. Novoselov, Composites Science and Technology 2012, 72, 1459.
[11] T. Hasan, Z. Sun, F. Wang, F. Bonaccorso, P. H. Tan, A. G. Rozhin, A. C. Ferrari, Advanced Materials 2009, 21, 3874.
[12] Z. Sun, T. Hasan, F. Torrisi, D. Popa, G. Privitera, F. Wang, F. Bonaccorso, D. M. Basko, A. C. Ferrari, Acs Nano 2010, 4, 803.
[13] M. Zhang, E. J. R. Kelleher, F. Torrisi, Z. Sun, T. Hasan, D. Popa, F. Wang, A. C. Ferrari, S. V. Popov, J. R. Taylor, Optics Express 2012, 20, 25077.
[14] O. Eksik, J. Gao, S. A. Shojaee, A. Thomas, P. Chow, S. F. Bartolucci, D. A. Lucca, N. Koratkar, Acs Nano 2014, 8, 5282.
[15] C. Y. Zhi, Y. Bando, C. C. Tang, H. Kuwahara, D. Golberg, Advanced Materials 2009, 21, 2889.
[16] A. Sorrentino, C. Altavilla, M. Merola, A. Senatore, P. Ciambelli, S. Iannace, Polymer Composites 2015, 36, 1124.
[17] K. Zhou, S. Jiang, C. Bao, L. Song, B. Wang, G. Tang, Y. Hu, Z. Gui, Rsc Advances 2012, 2, 11695.
[18] F. Xiaoming, K. Farhad, R. Vahid, S. Mariyappan, L. Masoud, J. Jacek, W. C. Robert, T. Eugene, P. Balaji, Nanotechnology 2015, 26, 261001.
[19] Y. Huang, Z. Luo, Y. Li, M. Zhong, B. Xu, K. Che, H. Xu, Z. Cai, J. Peng, J. Weng, Optics Express 2014, 22, 25258.
[20] Z. Luo, Y. Huang, M. Zhong, Y. Li, J. Wu, B. Xu, H. Xu, Z. Cai, J. Peng, J. Weng, Journal of Lightwave Technology 2014, 32, 4077.
[21] R. I. Woodward, E. J. R. Kelleher, R. C. T. Howe, G. Hu, F. Torrisi, T. Hasan, S. V. Popov, J. R. Taylor, Optics Express 2014, 22, 31113.
[22] M. Zhang, R. T. Howe, R. Woodward, E. R. Kelleher, F. Torrisi, G. Hu, S. Popov, J. R. Taylor, T. Hasan, Nano Res. 2015, 8, 1522.
[23] Z. Q. Luo, Y. Y. Li, M. Zhong, Y. Z. Huang, X. J. Wan, J. Peng, J. Weng, Photonics Res. 2015, 3, A79.

[24] Y. Hernandez, V. Nicolosi, M. Lotya, F. M. Blighe, Z. Sun, S. De, I. T. McGovern, B. Holland, M. Byrne, Y. K. Gun'Ko, J. J. Boland, P. Niraj, G. Duesberg, S. Krishnamurthy, R. Goodhue, J. Hutchison, V. Scardaci, A. C. Ferrari, J. N. Coleman, Nature Nanotechnology 2008, 3, 563.
[25] J. N. Coleman, M. Lotya, A. O'Neill, S. D. Bergin, P. J. King, U. Khan, K. Young, A. Gaucher, S. De, R. J. Smith, I. V. Shvets, S. K. Arora, G. Stanton, H.-Y. Kim, K. Lee, G. T. Kim, G. S. Duesberg, T. Hallam, J. J. Boland, J. J. Wang, J. F. Donegan, J. C. Grunlan, G. Moriarty, A. Shmeliov, R. J. Nicholls, J. M. Perkins, E. M. Grieveson, K. Theuwissen, D. W. McComb, P. D. Nellist, V. Nicolosi, Science 2011, 331, 568.
[26] E. Varrla, C. Backes, K. R. Paton, A. Harvey, Z. Gholamvand, J. McCauley, J. N. Coleman, Chemistry of Materials 2015, 27, 1129.
[27] K. R. Paton, E. Varrla, C. Backes, R. J. Smith, U. Khan, A. O'Neill, C. Boland, M. Lotya, O. M. Istrate, P. King, T. Higgins, S. Barwich, P. May, P. Puczkarski, I. Ahmed, M. Moebius, H. Pettersson, E. Long, J. Coelho, S. E. O'Brien, E. K. McGuire, B. M. Sanchez, G. S. Duesberg, N. McEvoy, T. J. Pennycook, C. Downing, A. Crossley, V. Nicolosi, J. N. Coleman, Nature Materials 2014, 13, 624.
[28] T. J. Nacken, C. Damm, J. Walter, A. Ruger, W. Peukert, RSC Advances 2015, 5, 57328.
[29] M. Lotya, Y. Hernandez, P. J. King, R. J. Smith, V. Nicolosi, L. S. Karlsson, F. M. Blighe, S. De, Z. M. Wang, I. T. McGovern, G. S. Duesberg, J. N. Coleman, Journal of the American Chemical Society 2009, 131, 3611.
[30] Y. T. Liang, M. C. Hersam, Journal of the American Chemical Society 2010, 132, 17661.
[31] A. B. Bourlinos, V. Georgakilas, R. Zboril, T. A. Steriotis, A. K. Stubos, Small 2009, 5, 1841.
[32] K. G. Zhou, N. N. Mao, H. X. Wang, Y. Peng, H. L. Zhang, Angewandte Chemie-International Edition 2011, 50, 10839.
[33] G. S. Bang, K. W. Nam, J. Y. Kim, J. Shin, J. W. Choi, S. Y. Choi, ACS Appl. Mater. Interfaces 2014, 6, 7084.
[34] M. Alsaif, S. Balendhran, M. R. Field, K. Latham, W. Wlodarski, J. Z. Ou, K. Kalantar-Zadeh, Sens. Actuator B-Chem. 2014, 192, 196.
[35] D. Hanlon, C. Backes, T. M. Higgins, M. Hughes, A. O'Neill, P. King, N. McEvoy, G. S. Duesberg, B. Mendoza Sanchez, H. Pettersson, V. Nicolosi, J. N. Coleman, Chemistry of Materials 2014, 26, 1751.
[36] P. Yasaei, B. Kumar, T. Foroozan, C. Wang, M. Asadi, D. Tuschel, J. E. Indacochea, R. F. Klie, A. Salehi-Khojin, Advanced Materials 2015, 27, 1887.
[37] Vishnu Sresht, Agilio A.H. Padua, Blankschtein, ACS Nano 2015, DOI: 10.1021/acsnano.5b02683.
[38] J. Kang, J. D. Wood, S. A. Wells, J.-H. Lee, X. Liu, K.-S. Chen, M. C. Hersam, Acs Nano 2015, 9, 3596.
[39] J. R. Brent, N. Savjani, E. A. Lewis, S. J. Haigh, D. J. Lewis, P. O'Brien, Chemical Communications 2014, 50, 13338.
[40] D. Hanlon, C. Backes, E. Doherty, C. S. Cucinotta, N. C. Berner, C. Boland, K. Lee, P. Lynch, Z. Gholamvand, A. Harvey, S. Zhang, K. Wang, G. Moynihan, A. Pokle, Q. M. Ramasse, N. McEvoy, W. J. Blau, J. Wang, G. Abellan, F. Hauke, A. Hirsch, S. Sanvito, D. D. O'Regan, G. S. Duesberg, V. Nicolosi, J. N. Coleman, Nature Communications 2015, in press.
[41] M. Naguib, O. Mashtalir, J. Carle, V. Presser, J. Lu, L. Hultman, Y. Gogotsi, M. W. Barsoum, Acs Nano 2012, 6, 1322.
[42] A. Harvey, C. Backes, Z. Gholamvand, D. Hanlon, D. McAteer, H. C. Nerl, E. McGuire, A. Seral-Ascaso, Q. M. Ramasse, N. McEvoy, S. Winters, N. C. Berner, D. McCloskey, J. Donegan, G. Duesberg, V. Nicolosi, J. N. Coleman, Chemistry of Materials 2015, DOI: 10.1021/acs.chemmater.5b00910.
[43] C. Backes, R. J. Smith, N. McEvoy, N. C. Berner, D. McCloskey, H. C. Nerl, A. O'Neill, P. J. King, T. Higgins, D. Hanlon, N. Scheuschner, J. Maultzsch, L. Houben, G. S. Duesberg, J. F. Donegan, V. Nicolosi, J. N. Coleman, Nature Communications 2014, 5, 4576.
[44] T. M. Higgins, D. McAteer, J. C. M. Coelho, B. M. Sanchez, Z. Gholamvand, G. Moriarty, N. McEvoy, N. C. Berner, G. S. Duesberg, V. Nicolosi, J. N. Coleman, Acs Nano 2014, 8, 9567.
[45] U. Khan, P. May, A. O'Neill, A. P. Bell, E. Boussac, A. Martin, J. Semple, J. N. Coleman, Nanoscale 2013, 5, 581.

[46] P. May, U. Khan, A. O'Neill, J. N. Coleman, Journal of Materials Chemistry 2012, 22, 1278.
[47] A. B. Bourlinos, V. Georgakilas, R. Zboril, T. A. Steriotis, A. K. Stubos, C. Trapalis, Solid State Commun. 2009, 149, 2172.
[48] P. May, U. Khan, J. M. Hughes, J. N. Coleman, Journal of Physical Chemistry C 2012, 116, 11393.
[49] J. Israelachvili, *Intermolecular and Surface Forces*, Academic press, 1991.
[50] S. Xie, O. M. Istrate, P. May, S. Barwich, A. P. Bell, U. Khana, J. N. Coleman, Nanoscale 2015, 7, 4443.
[51] O. M. Istrate, K. R. Paton, U. Khan, A. O'Neill, A. P. Bell, J. N. Coleman, Carbon 2014, 78, 243.
[52] U. Khan, A. O'Neill, H. Porwal, P. May, K. Nawaz, J. N. Coleman, Carbon 2012, 50, 470.
[53] W. Zhao, Z. Ghorannevis, L. Chu, M. Toh, C. Kloc, P.-H. Tan, G. Eda, ACS Nano 2012, 7, 791.
[54] A. Berkdemir, H. R. Gutierrez, A. R. Botello-Mendez, N. Perea-Lopez, A. L. Elias, C.-I. Chia, B. Wang, V. H. Crespi, F. Lopez-Urias, J.-C. Charlier, H. Terrones, M. Terrones, Sci. Rep. 2013, 3.
[55] T. M, D. J. Late, ACS Appl. Mater. Interfaces 2013, 6, 1158.
[56] X. Zhang, X.-F. Qiao, W. Shi, J.-B. Wu, D.-S. Jiang, P.-H. Tan, Chemical Society Reviews 2015, 44, 2757.
[57] H. Terrones, E. D. Corro, S. Feng, J. M. Poumirol, D. Rhodes, D. Smirnov, N. R. Pradhan, Z. Lin, M. A. T. Nguyen, A. L. Elias, T. E. Mallouk, L. Balicas, M. A. Pimenta, M. Terrones, Sci. Rep. 2014, 4.
[58] H. R. Gutiérrez, N. Perea-López, A. L. Elías, A. Berkdemir, B. Wang, R. Lv, F. López-Urías, V. H. Crespi, H. Terrones, M. Terrones, Nano Letters 2012, 13, 3447.
[59] E. Varrla, C. Backes, K. R. Paton, A. Harvey, Z. Gholamvand, J. McCauley, J. N. Coleman, Chemistry of Materials 2015, 27, 1129.
[60] M. Buzaglo, M. Shtein, S. Kober, R. Lovrincic, A. Vilan, O. Regev, Physical Chemistry Chemical Physics 2013, 15, 4428.
[61] Y. Lin, X. Ling, L. Yu, S. Huang, A. L. Hsu, Y.-H. Lee, J. Kong, M. S. Dresselhaus, T. Palacios, Nano Letters 2014, 14, 5569.
[62] K. F. Mak, K. He, C. Lee, G. H. Lee, J. Hone, T. F. Heinz, J. Shan, Nat Mater 2013, 12, 207.
[63] K. F. Mak, C. Lee, J. Hone, J. Shan, T. F. Heinz, Physical Review Letters 2010, 105, 136805/1.
[64] J. S. Ross, S. Wu, H. Yu, N. J. Ghimire, A. M. Jones, G. Aivazian, J. Yan, D. G. Mandrus, D. Xiao, W. Yao, X. Xu, Nat Commun 2013, 4, 1474.
[65] S. Mouri, Y. Miyauchi, K. Matsuda, Nano Letters 2013, 13, 5944.
[66] M. Rubinstein, R. H. Colby, *Polymer Physics*, Oxford University Press, Oxford 2003.
[67] N. Peimyoo, W. Yang, J. Shang, X. Shen, Y. Wang, T. Yu, ACS Nano 2014, 8, 11320.
[68] X. M. Zhang, L. Zhang, X. Y. He, J. T. Wu, Prog. Chem. 2014, 26, 1832.
[69] C. Teng, Y. Gao, X. Wang, W. Jiang, C. Zhang, R. Wang, D. Zhou, G. Xue, Macromolecules 2012, 45, 6648.
[70] D. Mao, Y. Wang, C. Ma, L. Han, B. Jiang, X. Gan, S. Hua, W. Zhang, T. Mei, J. Zhao, Sci. Rep. 2015, 5, 7965.
[71] C. Janisch, Y. Wang, D. Ma, N. Mehta, A. L. Elias, N. Perea-Lopez, M. Terrones, V. Crespi, Z. Liu, Sci. Rep. 2014, 4.
[72] M. O'Brien, N. McEvoy, T. Hallam, H.-Y. Kim, N. C. Berner, D. Hanlon, K. Lee, J. N. Coleman, G. S. Duesberg, Sci. Rep. 2014, 4, 7374.